J. Fluid Mech. (2001), *vol.* 431, *pp.* 161–188. Printed in the United Kingdom

Shock formation in the presence of entropy gradients

By HAO LIN AND ANDREW J. SZERI

Department of Mechanical Engineering, University of California at Berkeley, Berkeley, CA 94720-1740, USA

(Received 2 August 1999 and in revised form 14 September 2000)

The steepening of a normal compression wave into a shock in a homentropic flow field is understood well through the method of characteristics. In a non-homentropic flow field, however, shock formation from a compression wave is more complex. The effects of entropy (or sound speed) gradients on shock formation from a compression wave are determined using a wave front expansion in Cartesian and in spherical polar coordinates. The latter problem has application to the intense energy focusing of sonoluminescence, particularly when applied to a spherically collapsing gas. The principal result is an analytical criterion for the time and place of shock formation, for a wave propagating into a field of smoothly varying entropy.

1. Introduction

When a compression wave travels in a gas, it is well known that the disturbance tends to steepen as a consequence of nonlinearity. If, for example, the pressure at one end of a long cylinder containing gas is suddenly increased, the resulting compression wave will steepen until a shock forms. By use of the method of characteristics, it is possible to analyse such a problem when the compression wave is propagating into gas that is in a uniform state. In this simple case, the characteristics have a constant slope, and certain combinations of variables known as the Riemann invariants are constant along characteristics. These simplifications can be exploited to predict the time and place of shock formation.

In this paper, we consider the problem of a compression wave launched into a quiescent or radially collapsing gas where there is a smooth variation in the entropy ahead of the wave. Variable entropy is equivalent to variable sound speed, or density, or temperature, etc. Of interest to us is the rate of steepening of a compression wave in such a non-uniform environment.

This problem has application in the study of sonoluminescence, which is light emission from a spherically imploding bubble. It is thought that a compression wave in the gas interior, launched by the imploding surface, is important in concentrating energy near the bubble centre. How steep the compression wave becomes before it reflects from the origin is a key to determination of the peak temperatures and quantity of matter heated to extreme temperatures. In an earlier paper Vuong, Szeri & Young (1999) we argued that a compression wave can be prevented from steepening into a sharp shock before it reaches the bubble centre by an *adverse gradient in sound speed*. This gradient forms because: (i) the bubble collapse to one millionth the maximum volume causes enormous compression heating of the contents, and (ii) rapid heat conduction out of the bubble reduces the temperature near the wall.

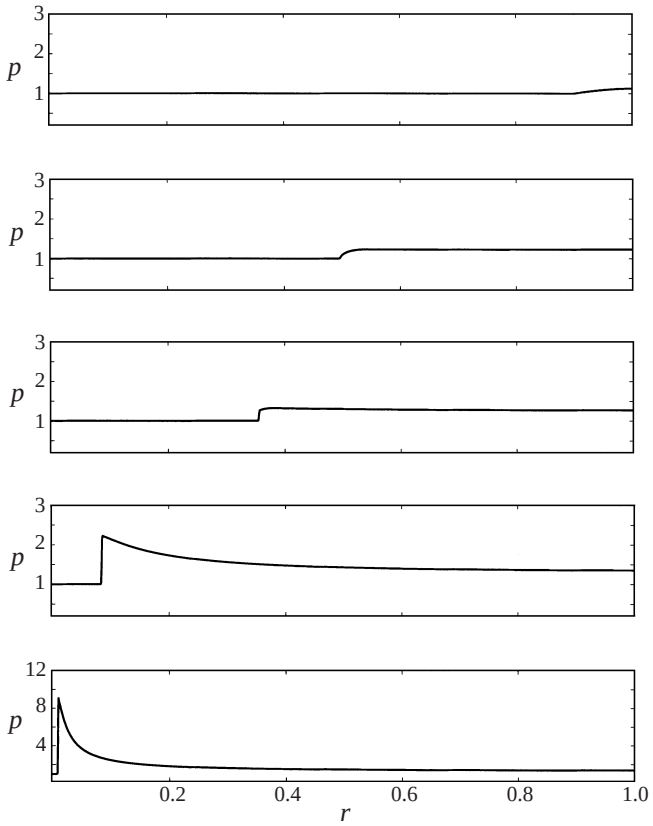

FIGURE 1. Evolution of an inwardly travelling spherical compression wave in a homentropic field. A shock forms well before it reaches the origin and increases rapidly in strength after formation. These results are from numerical solutions of the full nonlinear hyperbolic conservation laws, obtained using Clawpack (LeVeque 1997).

Hence, in the collapsed state when the compression wave is launched, the bubble contents are hot in the centre and cool near the wall. The compression wave thus travels inward into hotter and hotter gas with higher and higher sound speed. The leading edge of the compression wave outruns the trailing edge and the compression wave is prevented from steepening into a sharp shock. The consequence is that a large fraction of the bubble contents is heated over a time scale that compares well with time scales of sonoluminescence light emission (100 to 300 picoseconds, full width at half maximum). A theory which does not take into account thermal conduction (which leads to the adverse gradient in sound speed) yields sharp shocks which heat very little material to much more extreme temperatures over time scales that are too short when compared to experiment.

In the present work, we establish the validity of the mechanism just described – that of the sound speed (or entropy) gradient controlling shock formation. Although the gradient arises as a consequence of diffusive transport (as we argue in Vuong *et al.* 1999), the mechanism for controlling shock formation is purely hyperbolic. As an example of the phenomena with which we are concerned, we show the evolution of a compression wave in a spherical geometry in figures 1 and 2. The wave is travelling inward (right to left) and steepening on its way into a shock. One observes that the

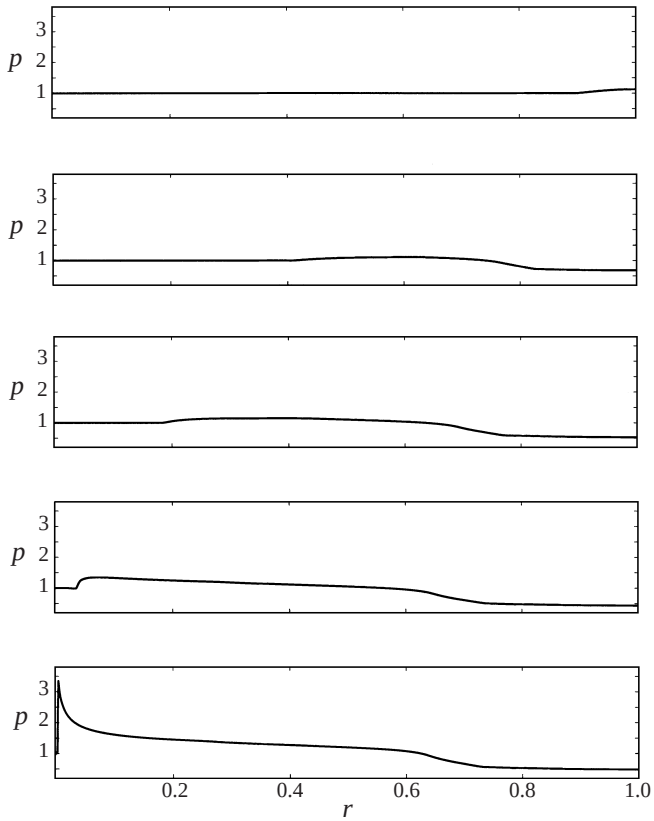

FIGURE 2. Evolution of the same compression wave as in figure 1 in a non-homentropic collapsing gas with an adverse sound speed (entropy profile) $a_0(r) = 4 - 3.5r^3$ and initial linear velocity field $v_0(r) = -2r$. Note that shock formation is delayed until very close to the origin, where (neglected) diffusion terms control the evolution, as explained in § 4.3. The pressure has been rescaled by the pressure at the centre.

shock forms rapidly in figure 1 – which corresponds to a homentropic field. In figure 2, the shock is weaker and its formation is delayed until very close to the origin. The factors responsible for the delay in shock formation in figure 2 are (i) the non-uniform entropy field into which the wave propagates, superposed (ii) on a radially collapsing flow. We develop an analytical criterion for when and where a shock will form in a spherically collapsing gas based on the initial conditions of a problem.

2. Nonlinear steepening of plane waves

First we consider for simplicity the case of plane waves. The spherically symmetric case shares many important features with plane waves. Furthermore, we restrict our considerations to a calorically perfect ideal gas. We shall review the characteristic formulation and one-dimensional wave motion before developing the shock formation criterion that is later illustrated with examples.

2.1. *Governing equations*

The equations of motion for isentropic flow are as follows. The mass balance is

$$\partial_t \rho + u\partial_x \rho = -\rho \partial_x u; \tag{2.1}$$

the balance of linear momentum is

$$\rho\partial_t u + \rho u\partial_x u = -\partial_x p; \tag{2.2}$$

the condition for isentropic flow requires

$$\partial_t s + u\partial_x s = 0. \tag{2.3}$$

These are supplemented by the equation of state $p = \rho RT$ and the expression for the sound speed $a^2 = \gamma RT$. Here $u(x,t)$ is the gas velocity, $p(x,t)$ is the pressure, $\rho(x,t)$ is the density, $T(x,t)$ is the temperature, $s(x,t)$ is the entropy, R is the gas constant and γ is the ratio of specific heats.

2.2. *Formulation on characteristics*

In the case where the entropy field is uniform, equations (2.1), (2.2), (2.3) can be conveniently analysed in characteristic coordinates as follows. There are two sets of characteristics in the (t,x)-plane, denoted C_+ and C_-; these are the graphs of $x_+(t)$ and $x_-(t)$, where

$$\dot{x}_+ = [u(x,t) + a(x,t)]_{x=x_+(t)}, \qquad \dot{x}_- = [u(x,t) - a(x,t)]_{x=x_-(t)}. \tag{2.4}$$

The dot denotes a simple time derivative. If we let $\mathrm{d}^+/\mathrm{d}t$ and $\mathrm{d}^-/\mathrm{d}t$ be the time derivatives along these two families of characteristics, i.e.

$$\frac{\mathrm{d}^+}{\mathrm{d}t} \equiv \partial_t + (u+a)\,\partial_x, \qquad \frac{\mathrm{d}^-}{\mathrm{d}t} \equiv \partial_t + (u-a)\,\partial_x, \tag{2.5}$$

then (2.1) and (2.2) are equivalent to

$$\frac{\mathrm{d}^+ u}{\mathrm{d}t} + \frac{1}{a\rho}\frac{\mathrm{d}^+ p}{\mathrm{d}t} = 0, \tag{2.6}$$

$$\frac{\mathrm{d}^- u}{\mathrm{d}t} - \frac{1}{a\rho}\frac{\mathrm{d}^- p}{\mathrm{d}t} = 0. \tag{2.7}$$

If we exploit the invariance of entropy, and eliminate p in favour of a, then we obtain the well-known evolution equations for the Riemann invariants $\Pi^+ \equiv u + 2a/(\gamma-1)$ and $\Pi^- \equiv u - 2a/(\gamma-1)$:

$$\frac{\mathrm{d}^+}{\mathrm{d}t}\Pi^+ = 0, \qquad \frac{\mathrm{d}^-}{\mathrm{d}t}\Pi^- = 0. \tag{2.8}$$

In the case where the entropy field is non-uniform, one obtains instead three characteristics (Courant & Friedrichs 1948). In addition to C_+ and C_- we have a third family of characteristics in the (t,x)-plane, the C_0 characteristics; these are the graphs of $x_0(t)$, where

$$\dot{x}_0 = [u(x,t)]_{x=x_0(t)}.$$

These are, of course, material curves. The Riemann invariants are no longer invariant in a non-homentropic flow, but instead we have on the two sound waves

$$\frac{\mathrm{d}^+}{\mathrm{d}t}\Pi^+ = \left(a^2/\gamma R\right)\,\partial_x s, \qquad \frac{\mathrm{d}^-}{\mathrm{d}t}\Pi^- = \left(a^2/\gamma R\right)\,\partial_x s, \tag{2.9}$$

and also (2.3): $\mathrm{D}s/\mathrm{D}t = 0$. In the latter equation, we have made use of $\mathrm{D}/\mathrm{D}t \equiv \partial_t + u\partial_x$.

For completeness, we note that non-uniformity in ρ, a or s does not drive a flow in a gas at uniform pressure and zero initial velocity. This can be shown from (2.3), (2.9).

2.3. *Shock formation*

We shall study the rate of steepening of the leading edge of a compression wave using a wave front expansion (Witham 1974). The disadvantage of this approach is that it neglects the possibility of shock formation in the middle of a wave, but it does shed light on the influence of the entropy gradient, etc. We note that no spherical wave is a pure compression or pure rarefaction wave (Landau & Lifshitz 1959); but we shall make reference to compression or rarefaction wave fronts.

The wave front expansion circumvents the impossible task of obtaining a global solution in closed form. For convenience we recast the Euler equations in terms of velocity u, sound speed a and entropy s, which can be obtained immediately from (2.9):

$$\partial_t a + u\partial_x a + \frac{\gamma - 1}{2} a\partial_x u = 0, \tag{2.10}$$

$$\partial_t u + u\partial_x u + \frac{2}{\gamma - 1} a\partial_x a - \frac{a^2}{\gamma R}\partial_x s = 0. \tag{2.11}$$

The expansion is based on the fact that for a hyperbolic system a discontinuity in the derivatives propagates on characteristics. For a wave with compact support travelling from left to right into a quiescent field, the wave front generally defines a discontinuity in derivatives of u. This wave front travels with the (fastest) right-travelling characteristic, which has position $x = F(t)$:

$$\dot{F}(t) = [a(x,t)]_{x=F(t)} \tag{2.12}$$

because $u(x,t)$ is always zero on the wave front in (2.4).

Although the diffusion terms are extremely small, they do eliminate instantaneously any C^1 discontinuity. However, the basic assumption of the wave front analysis is to follow such a discontinuity along a characteristic. The detailed structure of a shock has been much studied; there is superimposed on the solution of the hyperbolic conservation laws a thin transition layer within which the action of viscosity and thermal conduction is not negligible. The details of the viscosity and thermal conductivity are not so important as the two states on either side of a shock are known independently of the transport coefficients, and connected through thermodynamic relationships (Liepmann & Roshko 1957).

Before proceeding we remark that the wavefront expansion applies as well to the propagation of a discontinuity of order greater than one, e.g. to a wave that is C^1 but has a discontinuity in the second-order derivative. This has been done using singular surface theory by Shankar & Jain (1980). We refer the reader interested in extensions of the basic theory to Witham (1974), especially to the material on systems with more than two independent variables (§ 5.9), wave propagation on shocks (§ 8.5), and shock-shocks (§ 8.6).

In the neighbourhood of the wave front we define a new relative coordinate $\xi = x - F(t)$. In the new coordinate $\xi = 0$ denotes the wave front. Next we expand the dependent variables about the wave front for $\xi < 0$, and make use of the fact that in the quiescent field the sound speed and entropy are known functions $a_0(x)$ and $s_0(x)$:

$$a(\xi,t) = a_0(F(t)) + \xi a_1(t) + \tfrac{1}{2}\xi^2 a_2(t) + \cdots,$$

$$u(\xi,t) = \xi u_1(t) + \tfrac{1}{2}\xi^2 u_2(t) + \cdots,$$

$$s(\xi,t) = s_0(F(t)) + \xi s_1(t) + \tfrac{1}{2}\xi^2 s_2(t) + \cdots.$$

Note that $a_0(x)$ and $s_0(x)$ have been evaluated at $x = F(t)$. We remark that $a_0(x)$ and $s_0(x)$ cannot be specified independently, but are related by virtue of the fact that p is constant in the quiescent flow:

$$s_0'(x) = \frac{2\gamma R a_0'(x)}{(\gamma - 1)a_0(x)}. \tag{2.13}$$

This will be verified later for the expansion to be self-consistent.

The derivatives of the expansions with respect to time and space are required in what follows. First we write

$$\left[\frac{\partial}{\partial t}\right]_x = \left[\frac{\partial}{\partial t}\right]_\xi + \left[\frac{\partial \xi}{\partial t}\right]_x \frac{\partial}{\partial \xi} = \frac{\partial}{\partial t} - F'(t)\frac{\partial}{\partial \xi} = \frac{\partial}{\partial t} - a_0(F(t))\frac{\partial}{\partial \xi},$$

by use of (2.12). Now we substitute the expansions into (2.10), (2.11), (2.3) and equate terms of like order in ξ:

ξ^0:

$$a_1 - a_0' - \frac{\gamma - 1}{2}u_1 = 0, \tag{2.14}$$

$$u_1 + \frac{2}{\gamma - 1}a_1 - \frac{1}{\gamma R}a_0 s_1 = 0, \tag{2.15}$$

$$s_0' - s_1 = 0; \tag{2.16}$$

ξ^1:

$$\frac{\gamma - 1}{2}a_0 u_2 - a_0 a_2 = -\left(a_1' + \frac{\gamma + 1}{2}a_1 u_1\right), \tag{2.17}$$

$$-a_0 u_2 + \frac{2}{\gamma - 1}a_0 a_2 = -\left(u_1' + u_1^2 + \frac{2}{\gamma - 1}a_1^2\right) + \frac{1}{\gamma R}(a_0^2 s_2 + 2a_0 a_1 s_1), \tag{2.18}$$

$$s_1' - a_0 s_2 + u_1 s_1 = 0, \tag{2.19}$$

We proceed to obtain an evolution equation for $u_1(t)$ ($\partial_x u$ at the wave front) to judge when $u_1(t) \to \infty$, which is interpreted as shock formation. Note that the coefficient matrix for $u_2(t)$ and $a_2(t)$ is singular; this is always true if one expands a hyperbolic system about any one of its characteristics. (See Witham 1974 for a general proof.) We can therefore eliminate $u_2(t)$ and $a_2(t)$ by multiplying (2.17) by $2/(\gamma - 1)$ and adding the result to (2.18):

$$-\left(u_1' + u_1^2 + \frac{2}{\gamma - 1}a_1^2\right) + \frac{1}{\gamma R}(a_0^2 s_2 + 2a_0 a_1 s_1) - \frac{2}{\gamma - 1}\left(a_1' + \frac{\gamma + 1}{2}a_1 u_1\right) = 0. \tag{2.20}$$

To get to the final equation for $u_1(t)$ we need to eliminate a_1, s_1, s_2. This we do by use of (2.14), (2.16) and (2.19) in (2.20). After a considerable amount of algebra, we obtain an evolution equation for the slope of the leading edge of the compression wave, $u_1(t)$, in terms of the known sound field $a_0(F(t))$:

$$u_1'(t) + \tfrac{1}{2}a_0'(F(t))u_1(t) + \frac{\gamma + 1}{2}u_1^2(t) = 0. \tag{2.21}$$

The initial condition one requires is just the initial slope $\partial_x u$ at the wave front.

The nonlinear ODE (2.21) is a Bernoulli equation, which is readily transformed to a

linear ODE in the variable $u_1^{-1}(t)$. Thereafter an integrating factor yields the solution

$$\frac{1}{u_1(t)} = \left[\frac{1}{u_1(0)} + \frac{\gamma+1}{2}\int_0^t \exp\phi(\tau)\mathrm{d}\tau\right]\exp(-\phi(t)) \tag{2.22}$$

where

$$\phi(t) \equiv -\frac{1}{2}\int_0^t a_0'(F(\tilde{t}))\mathrm{d}\tilde{t}.$$

Together with the solution of (2.12), (2.22) constitutes an analytical solution for the time and place of shock formation at the leading edge of a plane wave propagating into a quiescent gas. The gas can be characterized by any variation of sound speed (or entropy) in the direction of travel.

Before turning to examples, we make a remark about the set of equations (2.14), (2.15), (2.16) that constitute the zeroth-order balance of ξ in the expansion. First, we note that the combination of (2.14), (2.15), (2.16) recovers (2.13) to order ξ^0.

The physical meaning of (2.14) is a little less apparent, as it involves a subtle link to the idea of *semi-simple waves*. It can be shown that equations (2.13), (2.14) and (2.16) are equivalent to the right-travelling semi-simple wave criterion developed in the Appendix. Hence, the (right-travelling) semi-simple wave condition is satisfied at the leading edge of a right-travelling wave propagating into a quiescent field. This recalls the result (*Fundamental Theorem, p. 61*) in Courant & Friedrichs (1948) which states: *The flow in a region adjacent to a region of constant state is a simple wave.* In the present language we can say the flow adjacent to a quiescent non-homentropic region is a semi-simple wave.

A final remark about (2.14) is that the relationship of $\partial_x u$ and $\partial_x a$ it implies is only true in general for $t > 0$. Mathematically equations (2.10), (2.11), (2.3) (or (2.9), (2.3)) are three equations for three unknowns fields: either (u, a, s) or (Π^+, Π^-, s). At $t = 0$ the three fields can be specified arbitrarily in a wave with compact support. The relation (2.14) is not necessarily true. However, as soon as the wave starts to propagate, (2.14) is satisfied exactly at the leading edge. This is analogous to the case of a simple wave with compact support: in the initial condition u and a can be specified arbitrarily, but once the wave starts to travel, at the wave front $\partial_x \Pi^- = 0$. Note that if $a_0' = 0$ in (2.14), this recovers the simple wave case.

2.4. *Examples*

Now we shall consider a few examples illustrative of the theory, both in homentropic and non-homentropic fields. A remark about dimensions is in order.

The variables may be regarded as dimensional. Also the variables can be alternatively considered as non-dimensionalized, with the two dimensionless numbers $[U][t]/[L]$ and $[p_0][T]/([\rho_0][U][L])$ equal to unity. Here $[U], [t], [L], [p_0]$ and $[\rho_0]$ are scales for velocity, time, length, pressure and density, respectively. In other words the velocity scale is chosen to be the length scale divided by the time scale, and the pressure is the density scale times velocity scale squared.

2.4.1. *Shock formation in homentropic flow*

In a homentropic flow ($a_0'(x) \equiv 0$), the solution (2.22) simplifies to

$$u_1(t) = \frac{u_1(0)}{1 + \frac{1}{2}(\gamma+1)u_1(0)t}.$$

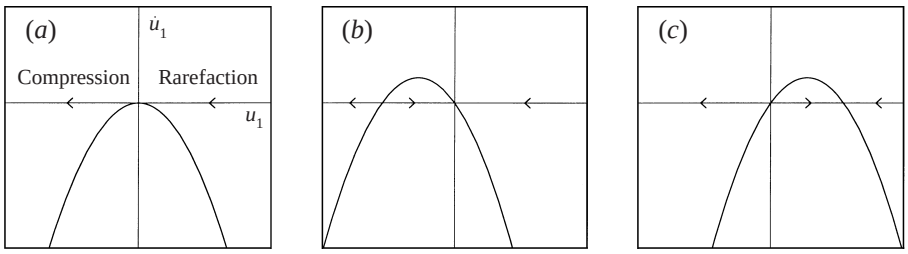

FIGURE 3. Rate of change of the slope ($\dot{u}_1$) versus the slope (u_1) at the leading edge of a right-travelling compression wave (equation (2.21)); the wave propagates into a domain where the wave speed (*a*) remains constant ($a_0'(x) = 0$), (*b*) increases ($a_0'(x) = 0.1$), and (*c*) decreases ($a_0'(x) = -0.1$).

From this, we see that $u_1(t)$ blows up for any negative $u_1(0)$ (i.e. compression wave) at time

$$t_B = \frac{2}{\gamma + 1} \frac{1}{|u_1(0)|},$$

thus recovering the classical result.

2.4.2. *Shock formation in non-homentropic flow*

Next we consider the simple but illuminating case of $a_0' \equiv \alpha$ constant. This yields an autonomous system for u_1 only. We find that two fixed points for (2.21) arise, rather than one as in the homentropic case. The fixed points are shown in figure 3. The solution (2.22) becomes

$$\frac{1}{u_1(t)} = \left(\frac{1}{u_1(0)} + \frac{\gamma + 1}{\alpha} \right) \mathrm{e}^{\alpha t/2} - \frac{\gamma + 1}{\alpha}. \tag{2.23}$$

We consider two separate cases $a_0' > 0$ and $a_0' < 0$. When $a_0' > 0$ the two fixed points are respectively negative and zero, thus all rarefaction wave fronts relax. The negative fixed point provides a separatrix for compression wave fronts. In other words, only strong enough compression waves will steepen into shocks; weaker ones will relax. Specifically, we find in this case that $u_1(t)$ blows up only for $u_1(0) < -\alpha(\gamma + 1)$, i.e. only for sufficiently steep compression waves. This has a nice physical interpretation: because the wave travels with local velocity $u + a$, a shock is harder to form in a field where a is greater in front than in a field where a is smaller in front. In terms of entropy, we can say by use of (2.13) that a positive entropy gradient ($s_0'(x) > 0$) is adverse to the formation of right-running shocks (however, the same entropy gradient promotes the formation of left-running shocks).

When $a_0' < 0$ one finds just the opposite: all compression wave fronts steepen into shocks, but there is an attracting point (i.e. a tendency toward a wave of permanent form) for all rarefaction waves.

We tested the analysis based on the wave front expansion using numerical methods to solve the full, nonlinear hyperbolic conservation laws (Clawpack, see LeVeque 1997). In figures 4 and 5 we show the evolution of the wave front steepness in the cases $a_0(x) = 1 - 0.1x$ and $a_0(x) = 0.1 + 0.1x$, respectively. The solid curves are from the analytical solution (2.23) and the dashed curves are the result of numerical integration of the full nonlinear hyperbolic conservation laws associated with the field equations (2.10), (2.11), (2.3). The initial waves with compact support satisfy the semi-simple wave relation $a\partial_x u - \partial_x p/\rho = 0$ for the wave to be right-travelling only. This is merely for ease of comparison with the analytical solution. In general an

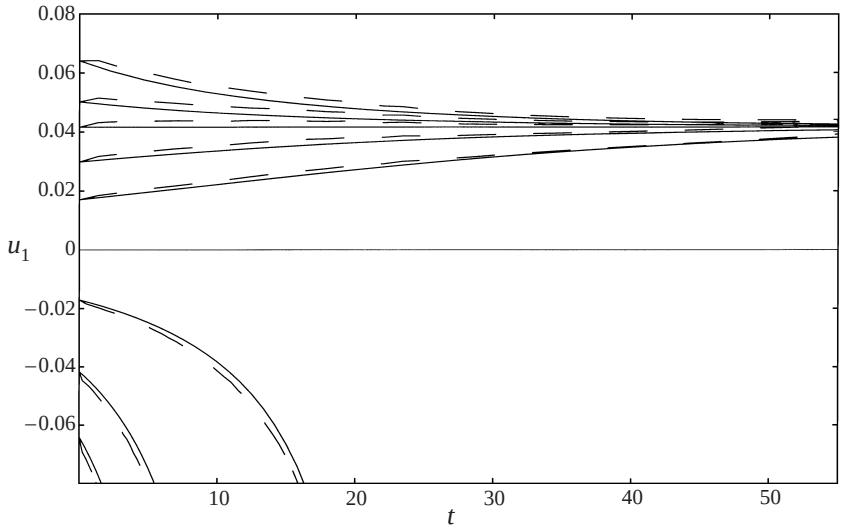

FIGURE 4. Plane wave front evolution when the sound speed decreases linearly in the direction of travel ($a_0(x) = 1 - 0.1x$). The slope of the leading edge of the wave is plotted against time. All compression waves ($u_1 < 0$) steepen into shocks; however all rarefaction waves ($u_1 > 0$) tend to the same leading edge slope. The dashed curves are from the numerical conservation law solution; note that there is some noise in the discontinuous leading edge slope. The solid curves are analytical solutions (2.23), developed by wavefront expansion.

arbitrary wave front propagating into a quiescent field adjusts itself to be semi-simple instantaneously after it takes off.

3. Nonlinear steepening of spherical waves

Now we turn to a case more relevant to sonoluminescence, but we do not yet include the spherically collapsing base flow. In a spherical geometry we assume that all the fields concerned are spherically symmetric, so that the problem remains one-dimensional. However, the focusing properties of the spherical geometry cause significant changes from the one-dimensional Cartesian case.

3.1. *Governing equations*

To distinguish the spherical case from the Cartesian case we denote the velocity by v. The balances of mass, momentum and energy are the same as those of the Cartesian case, except for an extra source term in the continuity equation:

$$\partial_t \rho + v\partial_r \rho + \rho \partial_r v = -\frac{2\rho v}{r}, \tag{3.1}$$

$$\rho \partial_t v + \rho v \partial_r v + \partial_r p = 0, \tag{3.2}$$

$$\partial_t s + v\partial_r s = 0. \tag{3.3}$$

The source term arises due to the fact that in a spherical geometry the surface area is a varying function of r. Also there are the equation of state and the expression for sound speed, which remain the same.

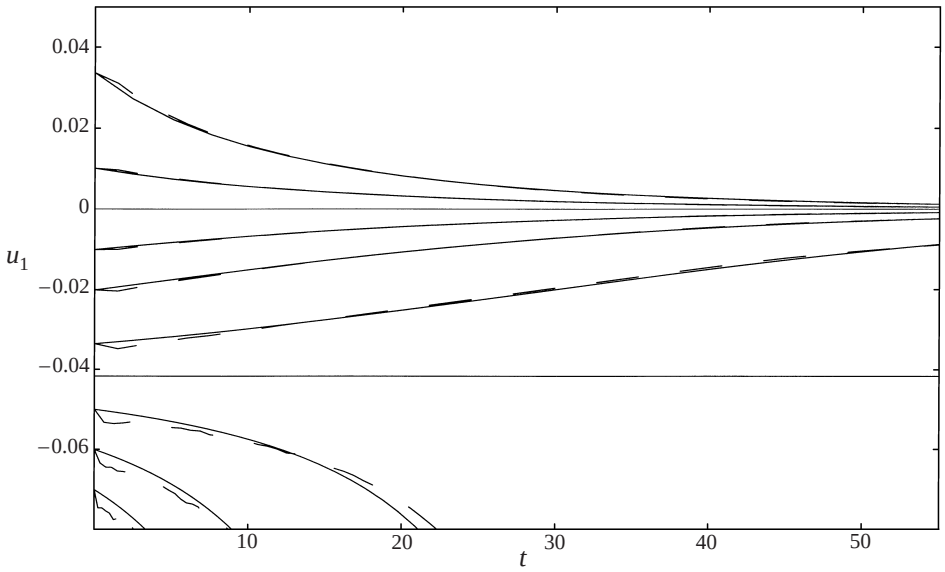

FIGURE 5. Plane wave front evolution when the sound speed increases linearly in the direction of travel ($a_0(x) = 0.1 + 0.1x$). All rarefaction waves ($u_1 > 0$) and sufficiently weak compression waves ($u_1 < 0$) relax to zero leading edge slope. A strong enough compression wave ($u_1(0) < -0.04$) becomes a shock. The curves are computed in same way as figure 4.

3.2. *Formulation on characteristics*

Because the source term in (3.1) does not appear in the derivatives, the hyperbolic structure carries over from the Cartesian case, except for source terms:

$$\frac{\mathrm{d}^+ v}{\mathrm{d}t} + \frac{1}{\rho a}\frac{\mathrm{d}^+ p}{\mathrm{d}t} = -\frac{2av}{r}, \qquad \frac{\mathrm{d}^- v}{\mathrm{d}t} - \frac{1}{\rho a}\frac{\mathrm{d}^- p}{\mathrm{d}t} = \frac{2av}{r},$$

where $\mathrm{d}^+/dt = \partial_t + (v + a)\partial_r$ and $\mathrm{d}^-/dt = \partial_t + (v - a)\partial_r$. One should note that the concept of a simple wave is no longer available even when the flow is homentropic. The Riemann invariants are no longer invariant along the characteristics even when s is uniform, owing to the extra source terms arising from geometry, as can be seen from the evolution equations

$$\frac{\mathrm{d}^+ \Pi^+}{\mathrm{d}t} = \frac{a^2}{\gamma R}\frac{\partial s}{\partial r} - \frac{2av}{r}, \qquad \frac{\mathrm{d}^- \Pi^-}{\mathrm{d}t} = \frac{a^2}{\gamma R}\frac{\partial s}{\partial r} + \frac{2av}{r}.$$

Here Π^+ and Π^- are, as before, $\Pi^+ = v + 2a/(\gamma - 1)$ and $\Pi^- = v - 2a/(\gamma - 1)$.

3.3. *Shock formation*

We study a wave propagating inwardly to the centre of the coordinate system, so that the wave front $r = F(t)$ propagates along a C_- characteristic. Again we assume a quiescent flow in front of the wave. Hence $v = 0$ at the wave front which travels inwardly with local sound speed $a(F(t))$. A typical initial condition is shown in figure 6.

We make use of the same expansion technique used in § 2.3. As before, the goal is to develop an evolution equation for $v_1(t)$, which is $\partial_r v$ at the wave front. We shall

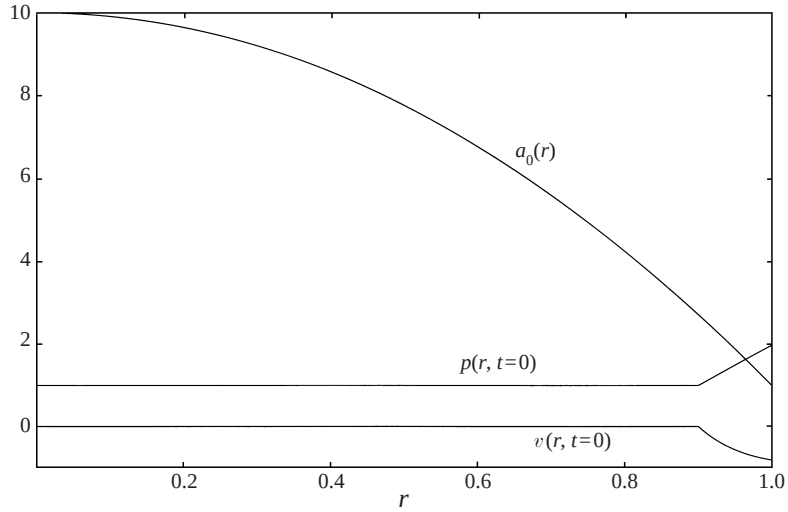

FIGURE 6. Example initial conditions for an inwardly travelling spherically symmetric compression wave. The sound speed varies by one order of magnitude, increasing ahead of the wave. Such a sound speed gradient is representative of those in the interior of sonoluminescence bubbles after the inertial collapse. The gas is quiescent ahead of the wave.

avoid the lengthy development and give the resulting ODE for $v_1(t)$,

$$v_1' - \left(\frac{a_0'(F(t))}{2} + \frac{a_0(F(t))}{F(t)} \right) v_1 + \frac{\gamma + 1}{2} v_1^2 = 0. \tag{3.4}$$

This is again a Bernoulli equation and has a formal solution (2.22) with $\phi(t)$ defined instead as

$$\phi(t) \equiv \int_0^t \left(\frac{a_0'(F(\tilde{t}))}{2} + \frac{a_0(F(\tilde{t}))}{F(\tilde{t})} \right) \mathrm{d}\tilde{t}. \tag{3.5}$$

Here $a_0(r)$ is the sound speed of the quiescent field; $F(t)$ is the wave front position defined as $\dot{F}(t) = -a_0(F(t))$; and γ is the ratio of specific heats.

3.4. *Examples*

Together with the solution for the wave front position, (2.22), (3.5) is an analytical solution for the slope of the leading edge of a spherical wave propagating into the centre of an otherwise quiescent region with any sound speed (or entropy) profile. In what follows we illustrate this result with some examples.

3.4.1. *Shock formation in homentropic flow*

To analyse the physical meaning of (2.22), (3.5), we first consider the homentropic case, i.e. when $a_0(r) \equiv a$ constant. The wave front position can then be expressed as $F(t) = r_0 - at$, with r_0 denoting the initial position. The solution in explicit form is

$$\frac{1}{v_1(t)} = \left[\frac{1}{v_1(0)} - \frac{(\gamma + 1) r_0}{2a} \ln \frac{r_0 - at}{r_0} \right] \frac{r_0 - at}{r_0}, \tag{3.6}$$

which recovers equation (10) of Greenspan & Nadim (1993). For convenience we define the time at which the wave front reaches the centre ($r = 0$) as t_c: in the present case $t_c = r_0/a$. Note that it only makes sense to consider the time period $0 < t < t_c$

in the spherical case; an account of the wave reflection at the origin is outside the scope of our analysis.

From (3.6) we see that when t varies from 0 to t_c the second term in the brackets varies from 0 to $+\infty$, which means that if $v_1(0)$ is negative, $1/v_1(t)$ always has a zero somewhere between $t = 0$ and $t = t_c$. Therefore in a homentropic field an inward-travelling compression wave (corresponding to $v_1(0) < 0$) always evolves into a shock wave before it reaches the origin.

3.4.2. *Shock formation in non-homentropic flow*

We note that although the system of equations (2.22), (3.5) is a solution for the slope of the leading edge of the wave, it is not practical to discuss the solution in complete generality. As an example of a specific non-homentropic case, we consider the simplest possible variation of sound speed with r, which can be motivated also by the Taylor expansion of a general $a(r)$ about $r = 0$:

$$a_0(r) = A + Br^2 + \cdots, \tag{3.7}$$

where A and B are constants. Note that A must be positive, and that the first derivative vanishes as is required in view of the coordinate singularity at the origin. In this consideration Br^2 can be regarded as the leading term in an expansion. Note that we might choose higher-order polynomials for a better representation of the sound field, such as we do below in the example of figure 13(*b*). There, $A + Br^8$ is used to represent an almost uniform sound field with a sharp decrease in a small region attached to the bubble wall.

A shock always forms either before or just as the wave reaches the origin. This is simply because, as $r \to 0$, the expansion (3.7) is dominated by the constant A, and thus recovers the homentropic case. However, a more detailed study shows that if the compression wave is weak or the constant B is large and negative enough, the shock forms only very close to the origin, which is well within the region where diffusion dominates (see the discussion below in § 4.3).

Hence, although the right kind of entropy (or sound speed) gradient cannot prevent shock formation in a spherical geometry, it *is* able to delay the shock formation until it gets very close to the origin – where diffusion is the dominating phenomenon.

To illustrate we take $A = 10$ and $B = -9$. All the inward-travelling waves we discuss below are compressions except for those in figure 9. Such a sound speed gradient is similar to that computed in the interior of a sonoluminescence bubble (Vuong *et al.* 1999). As in the Cartesian case, the numerical simulation is developed using Clawpack.

As initial conditions we take v and p as shown in figure 6 in the domain of $r > 0.9$. The fields satisfy $a\partial_r v - \rho^{-1}\partial_r p = 0$ in order for the wave to be inward-travelling only, for convenience.

In figures 7–9, we plot the inverse of the steepness $1/v_1(t)$ parametrically against the location of the wave front $r = F(t)$. As $1/v_1 \to \infty$, the wave front is an increasingly weak rarefaction; as $1/v_1 \to -\infty$, the wave front is an increasingly weak compression. A compression wave steepening into a shock approaches $1/v_1 = 0$ through negative values (figures 7 and 8); a rarefaction wave steepening into a shock approaches $1/v_1 = 0$ through positive values (figure 9). If the locus of front location and inverse steepness reaches $1/v_1 = 0$ first then there is shock formation at some finite r (three upper sets of curves in figure 8), while if it reaches $r = 0$ first there is no shock formation before the wave front reaches the origin.

In figure 7 we show that relatively weak compression waves, under the influence

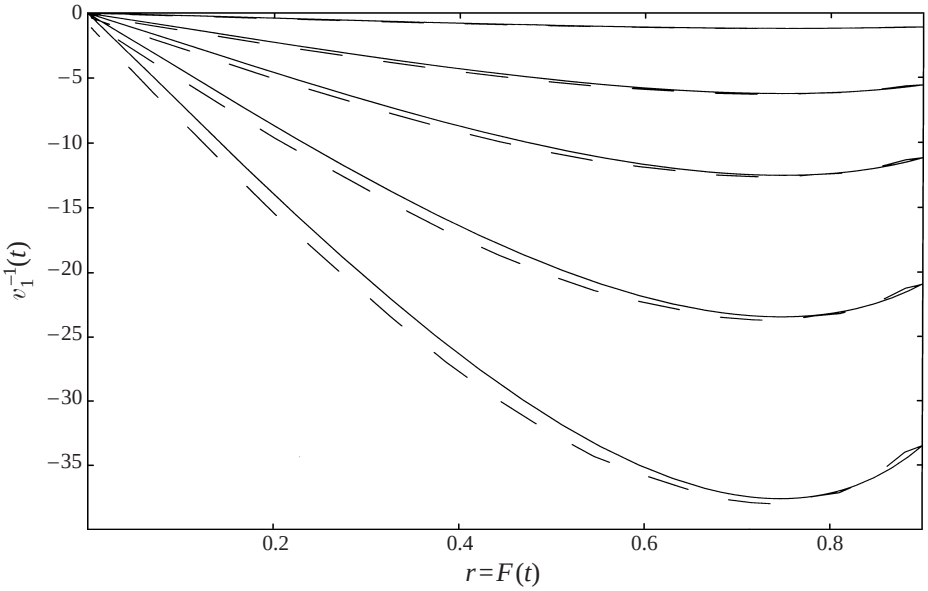

FIGURE 7. Evolution of the slope of the wave front (v_1) of an inward-travelling compression wave plotted parametrically against the position of the wave fronts. The wave fronts move from right to left. These weaker compression waves only just steepen into shocks at the centre of the coordinate system. They are prevented from steepening more quickly by the gradient in entropy (or sound speed $a_0(r) = 10 - 9r^2$) in the quiescent gas into which they travel. The dashed curves are the numerical result of integrating the conservation laws. The solid curves are the analytical result of the wavefront expansion.

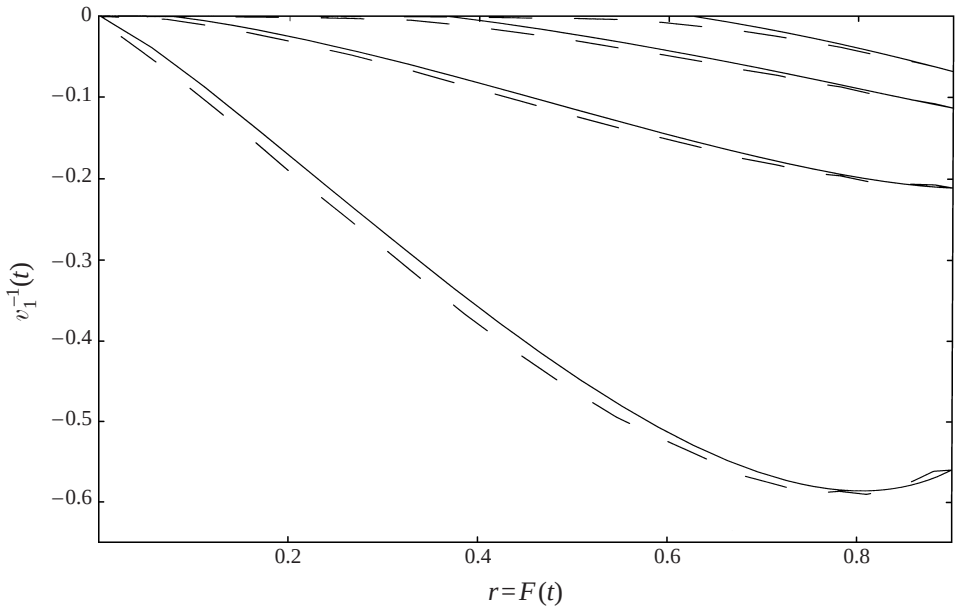

FIGURE 8. When propagating into the same quiescent entropy field as figure 7, stronger compression waves rapidly steepen into shocks – well before reaching the origin (three upper sets of the curves). Note that the conservation law solver (dashed curve) cannot resolve a discontinuity at a shock front; hence the dashed curves can only asymptotically approach $1/v_1 = 0$.

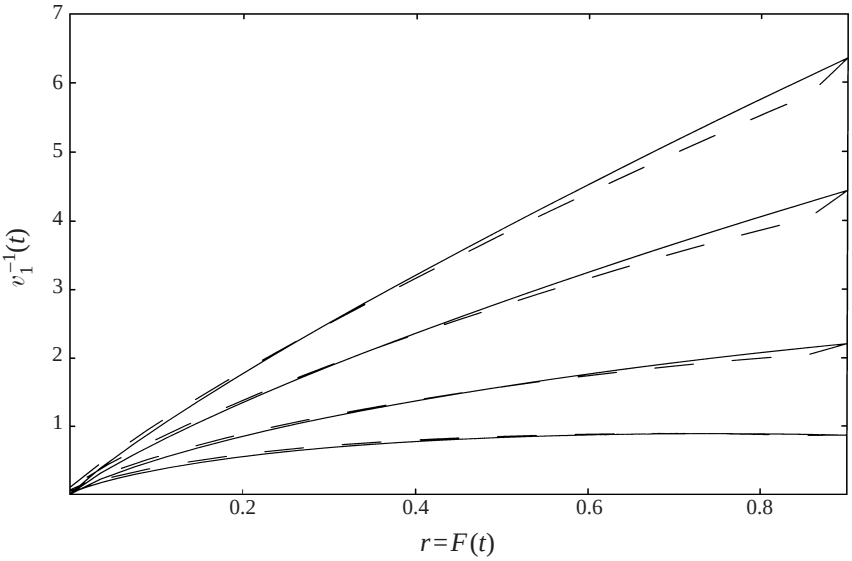

FIGURE 9. An illustration of rarefaction wavefronts propagating inward into a homentropic field, steepening as they go into infinitesimal shocks at the origin (in the absence of diffusion).

of the steep negative sound speed gradient, first relax somewhat and then steepen on their way into the origin. The waves evolve into infinitesimal shocks as they reach the origin.

In figure 8 we show the fate of stronger compression waves. The three upper sets of solid curves (analytical results) show that shocks form at a finite distance from the origin. The numerical solver for the conservation laws cannot quite resolve the shock, of course. In the numerical simulation the shock is captured by a jump of values on two neighbouring cells, so the simulation curves only asymptotically approach $1/v_1(t) = 0$.

The case $B > 0$ is less interesting because then the physical conditions in the quiescent gas favour shock formation as does the geometric term. Hence shocks form faster than for the homentropic case. Only for negative B is there a competition between the natural tendency to shock formation and the adverse sound speed gradient.

In figure 9 we illustrate the curious result that even inward-travelling rarefaction wave fronts steepen in the homentropic case in a spherical geometry. This is not observed in the Cartesian geometry. We note that the extension of this phenomenon to the formation of a 'rarefaction shock' does not occur, for two reasons. First, rarefaction shocks are susceptible to mechanical instability (Zel'dovich & Raizer 1966). Second, in the inviscid theory infinitesimal rarefaction shocks form just as the waves reach the bubble centre; this would always be eliminated by diffusion in a real situation. We present the details concerning the importance of diffusion near the origin in §4.3. Notwithstanding those arguments, it is nevertheless true that the spherical geometry provides a steepening mechanism even for rarefaction waves.

4. Nonlinear steepening of spherical waves in a collapsing gas

In this section, we turn to the analysis of shock formation from a wave propagating in a spherically collapsing gas. In a collapsing sonoluminescence bubble, the flow on

which the wave propagates is linear in r rather than quiescent. In the following we develop the base flow, then we explore the evolution of inwardly travelling waves on this base flow with the wave front expansion technique.

4.1. *Base flow*

Our major sources of numerical observations are from Storey & Szeri (2000) and Chu (1996). In Storey & Szeri (2000), in spite of all the complicated physics in a collapsing bubble, the velocity field prior to wave formation remains linear to a good approximation. Following Chu (1996) we assume that the flow inside the bubble is 'homologous', i.e. all the 'thermodynamic variables factorize into products of a time-dependent factor and another factor depending only on the scaled spatial variable $r/R(t)$' where $R(t)$ is the bubble radius. In what follows, we assume a linear velocity field and derive the possible constraints on thermodynamic variables. This will later be used as an exact base flow solution on which is superposed the compression wave of interest.

We start with $v(r,t) = \alpha(t)r$. Individual material points evolve according to

$$r = r_0 \mathrm{e}^{\beta(t)}.$$

Here $\beta(t) \equiv \int_0^t \alpha(t)\mathrm{d}t$ and r_0 is the initial condition. Next we substitute the linear form of velocity into the continuity equation (3.1). The result can be integrated to obtain

$$\rho = \rho_0(r_0)\mathrm{e}^{-3\beta(t)},$$

where $\rho_0(r_0)$ is the density field at time $t = 0$. Note that this is in Lagrangian form. In an Eulerian representation

$$\rho(r,t) = \rho_0(r\mathrm{e}^{-\beta(t)})\mathrm{e}^{-3\beta(t)}.$$

Next we solve for the pressure from the energy equation. We rewrite (3.3) in the form

$$\frac{\mathrm{D}p}{\mathrm{D}t} - a^2\frac{\mathrm{D}\rho}{\mathrm{D}t} = 0.$$

We substitute for ρ and v and solve for p to obtain

$$p(r,t) = p_0(r_0)\mathrm{e}^{-3\gamma\beta(t)},$$

where p_0 is the initial distribution of pressure. Finally we consider the momentum equation. With expressions for v, ρ and p substituted into (3.2) we obtain

$$\alpha'(t) + \alpha^2(t) = -\frac{\partial p_0/\partial r_0}{r_0\rho_0(r_0)}\mathrm{e}^{(1-3\gamma)\beta(t)}. \tag{4.1}$$

Note that because α and β are functions of time only, the factor $(\partial p_0/\partial r_0)/(r_0\rho_0(r_0))$ must be a constant for the ansatz to work. This is the desired constraint on the initial pressure and density fields. The constant turns out to control the growth or decay of $\alpha(t)$, and consequently the whole base flow.

To satisfy the constraint there are many possibilities. For example, p_0 could be quadratic and ρ_0 constant. In this paper, we focus on the case of relevance to sonoluminescence: uniform pressure p_0. See Prosperetti (1991) for a discussion of when the pressure may be regarded as uniform.

An immediate advantage of uniform p_0 is that it automatically satisfies (4.1) without any constraint on the initial density field (or sound field, or entropy field). The velocity

gradient $\alpha(t)$ has a simple solution

$$\alpha(t) = \frac{\alpha_0}{\alpha_0 t + 1}, \tag{4.2}$$

where α_0 is the initial condition for α. Note that if $\alpha_0 < 0$ (the contracting case of interest), the velocity gradient tends to ∞ as $t \to -1/\alpha_0$. This has no effect on the shock formation analysis, because the compression wave always travels faster than a material point by the speed of sound and reaches the bubble centre before the base flow solution (4.2) ceases to make sense, as we shall see in the following analysis. With (4.2) the exact solution is fully specified in an Eulerian representation:

$$v_e = \frac{\alpha_0 r}{\alpha_0 t + 1}, \tag{4.3}$$

$$\rho_e = \rho_0 \left(\frac{r}{\alpha_0 t + 1} \right) \frac{1}{(\alpha_0 t + 1)^3}, \tag{4.4}$$

$$p_e = p_0 \frac{1}{(\alpha_0 t + 1)^{3\gamma}}, \tag{4.5}$$

$$a_e = a_0 \left(\frac{r}{\alpha_0 t + 1} \right) (\alpha_0 t + 1)^{(3-3\gamma)/2}, \tag{4.6}$$

where $a_0 \equiv (\gamma p_0/\rho_0)^{1/2}$, and p_0 now denotes a constant rather than a function of r_0. In addition we have the trajectories $r(t) = r_0(\alpha_0 t + 1)$ for arbitrary r_0. Hence the bubble wall, which we could ascribe to any material point, evolves as $R(t) = R_0(\alpha_0 t + 1)$. Together (4.3), (4.4), (4.5) constitute an exact solution of the Euler equations. This is the base flow; superposed on this flow will be a compression wave whose fate we wish to discover.

4.2. *Shock formation*

Again we explore the steepening of a compression wave with the wave front expansion technique. A pressure wave of first-order discontinuity is launched into the collapsing (or expanding) gas. The wave front travels along the characteristic that is defined by $\dot{F}(t) = [v_e(r,t) - a_e(r,t)]_{r=F(t)}$. As in previous sections a wave front variable $\xi = x - F(t)$ is defined and all the dependent variables are expanded on the wave front about the exact solution:

$$v = v_e(F(t),t) + \xi v_1(t) + \tfrac{1}{2}\xi^2 v_2(t) + \cdots,$$

$$\rho = \rho_e(F(t),t) + \xi \rho_1(t) + \tfrac{1}{2}\xi^2 \rho_2(t) + \cdots,$$

$$p = p_e(F(t),t) + \xi p_1(t) + \tfrac{1}{2}\xi^2 p_2(t) + \cdots.$$

These expansions are substituted into the governing equations to obtain the evolution equation for the wave front. In this case $p_1 \equiv [\partial p/\partial r]_{r=F(t)}$ turns out to be a better variable to use in the wave front analysis. We skip the lengthy calculation and write the resulting evolution equation in terms of $p_1(t)$:

$$p_1'(t) + \left[\tfrac{9}{4}(\gamma+1)\alpha(t) - \frac{a_e(F(t),t)}{F(t)} - \frac{3}{2}\frac{\partial a_e}{\partial r}(F(t),t) \right] p_1(t) - \frac{\gamma+1}{2}\frac{1}{\rho_e a_e} p_1(t)^2 = 0. \tag{4.7}$$

This equation is formally identical to that of the spherical quiescent case except for the new term $(9/4)(\gamma+1)\alpha(t)$ in the coefficient of p_1. The physical origin of each of the three terms in the coefficient of p_1 is evident: $(9/4)(\gamma+1)\alpha(t)$ is associated

with the base flow contraction/expansion; $-a_e/F(t)$ is the geometric factor; and $-(3/2)\,\partial a_e/\partial r$ is the term associated with the sound speed gradient. The influence of the first coefficient on shock formation depends on the sign of α: if $\alpha > 0$ (expanding base flow) the first term slows the steepening of the wave front; otherwise it speeds shock formation. Care must be taken in interpretation of such statements, however, because the sign and magnitude of $\alpha(t)$ also affect strongly the position of the wave front, as we show below.

The three coefficients of $p_1(t)$ in (4.7) eventually tend to ∞ as time increases; however, the geometric term always becomes singular faster than the other two, because it does so when the wave front reaches the geometric centre. The other two coefficients tend to ∞ when $\alpha(t)$ does. As we mentioned before, the wave front always reaches the centre before $\alpha(t)$ goes to $-\infty$. Hence the geometric term is always dominant as the wave propagates into the centre. We therefore conclude that shock formation is inevitable, due to the geometric factor.

As in the previous sections equation (4.7) has a formal solution as a Bernoulli equation. This is difficult to analyse in general because the solution depends largely on specific forms of the sound field. However, when $\gamma = 5/3$ a special structure obtains with the consequence that strong conclusions can be built around this case.

4.2.1. *Special structure in the case* $\gamma = 5/3$

Equation (4.7) possesses a very interesting similarity structure only in the case $\gamma = 5/3$. To see this we rewrite the system in terms of $q(t) \equiv 1/p_1(t)$:

$$q'(t) = \left(\tfrac{9}{4}(\gamma+1)\alpha(t) - \frac{a_e(F,t)}{F} - \frac{3}{2}\frac{\partial a_e}{\partial r}(F,t)\right) q(t) - \frac{\gamma+1}{2}\frac{1}{\rho_e a_e}, \tag{4.8}$$

$$F'(t) = v_e(F,t) - a_e(F,t). \tag{4.9}$$

Now we scale q with $(\alpha_0 t + 1)/p_e$ and F with $\alpha_0 t + 1$, and name the scaled variables $\tilde{q}$ and $\tilde{F}$; the system then becomes

$$\tilde{q}'(t) = \left(\frac{5-3\gamma}{4}\alpha(t) - \frac{a_e(F,t)}{F} - \frac{3}{2}\frac{\partial a_e}{\partial r}(F,t)\right) \tilde{q}(t) - \frac{\gamma+1}{2\gamma}\frac{a_e}{\alpha_0 t + 1}, \tag{4.10}$$

$$\tilde{F}'(t) = -\frac{a_e(F,t)}{\alpha_0 t + 1}. \tag{4.11}$$

Clearly when $\gamma = 5/3$ the coefficient of $\alpha(t)$ in equation (4.10) disappears naturally. If we recall the functional form (4.6) of a_e and divide (4.10) by (4.11) we obtain

$$\frac{\mathrm{d}\tilde{q}}{\mathrm{d}\tilde{F}} = \left(\frac{1}{\tilde{F}} + \frac{3}{2}\frac{\partial \ln a_0(\tilde{F})}{\partial \tilde{F}}\right) + \frac{\gamma+1}{2\gamma}. \tag{4.12}$$

Equation (4.12) is invariant with respect to changes in α_0, hence a parametric plot of $\tilde{q}(t)$ vs. $\tilde{F}(t)$ is independent of the contraction/expansion rate.

In figure 10, we demonstrate this α_0-invariance. In figure 10(*a*) the traces of three steepening wave fronts are shown, with $\alpha_0 = 0, -2$ and -4 and all else equal. The initial sound field and pressure field are taken to be $a_0(r) = 4 - 3r^3$ and $p_0 = 1$, respectively. Compression waves of the same magnitude are launched from position $r = 0.9$. Note that with increasing contraction the curves move more quickly along the horizontal axis. This is because contraction contributes directly to the speed of the wave front (see (4.9)). In figure 10(*b*) under scaling the three curves collapse onto a single curve. Because the scaling is trivial for $\alpha_0 = 0$ given $p_0 = 1$, the quiescent curve remains unchanged. All the other curves collapse onto it.

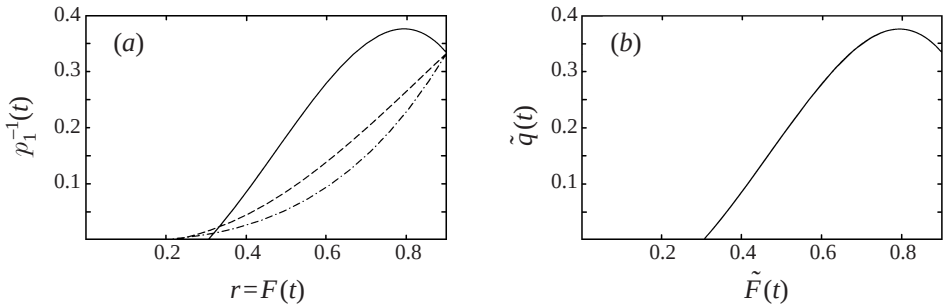

FIGURE 10. Evolution of an inwardly travelling compression wave front in three cases in physical variables (*a*), and in scaled variables (*b*). The wave fronts move from right to left. In (*a*), the solid curve is for a quiescent base flow ($\alpha = 0$), the dashed curve is for a mild collapse $\alpha = -2$, and the dot-dashed curve is for a stronger collapse $\alpha = -4$. In (*b*) all three curves reduce to a single curve in the scaled variables when $\gamma = 5/3$.

This result is very powerful because if we want to calculate the position and time of shock formation for any initial contraction/expansion α_0, we need only determine the answer in the quiescent case. The non-quiescent case can be easily recovered from the scaling. Suppose in a quiescent case a shock forms at position R_0 and time t_0, then for some contraction ratio $\alpha_0 = c_1$, the scaled spatial variable would yield the shock formation position $\tilde{R}_1 = \tilde{R}_0 = R_0$. Thus in order to calculate the un-scaled position R_1, we simply multiply $\tilde{R}_1$ by $c_1 t_1 + 1$. Here t_1 is the time of shock formation for the $\alpha_0 = c_1$ case. Note we did not scale time, so t_1 should be the time for $\tilde{F}$ to reach the position R_0 and different from t_0, as we see from equation (4.11).

Next we calculate t_1 assuming t_0 is known. Integration of (4.11) with $\alpha_0 = 0$ and c_1 respectively yields

$$t_0 = -\int_{R_i}^{R_0} \frac{1}{a_0(\tilde{F})} \mathrm{d}\tilde{F},$$

$$\frac{1}{c_1(c_1 t_1 + 1)} - \frac{1}{c_1} = \int_{R_i}^{R_0} \frac{1}{a_0(\tilde{F})} \mathrm{d}\tilde{F}.$$

Here, R_i is the position of the wave front at $t = 0$. Elimination of the integral yields

$$t_1 = \frac{t_0}{1 - c_1 t_0}.$$

The expression for R_1 thus follows:

$$R_1 = \frac{R_0}{1 - c_1 t_0}. \tag{4.13}$$

This is a very useful formula: it represents clearly the influence that the contracting/expanding base flow has on the shock formation process. If $c_1 \to 0$, R_1 naturally tends to R_0; on the other hand for an infinitesimal shock, i.e. a shock formed close enough to the origin for no fetch to develop, we simply make the contraction rate $\alpha_0 = c_1$ large and negative. For rapid shock formation, a wave should be launched into an *expanding* bubble.

In figure 5 of Vuong *et al.* (1999), there is an excellent example of the latter. There, a compression wave is launched from the wall of a collapsing bubble, reflects from the centre, and again from the wall. A shock forms only in the third leg of the journey, when the compression wave is travelling inward into an expanding gas. This is true

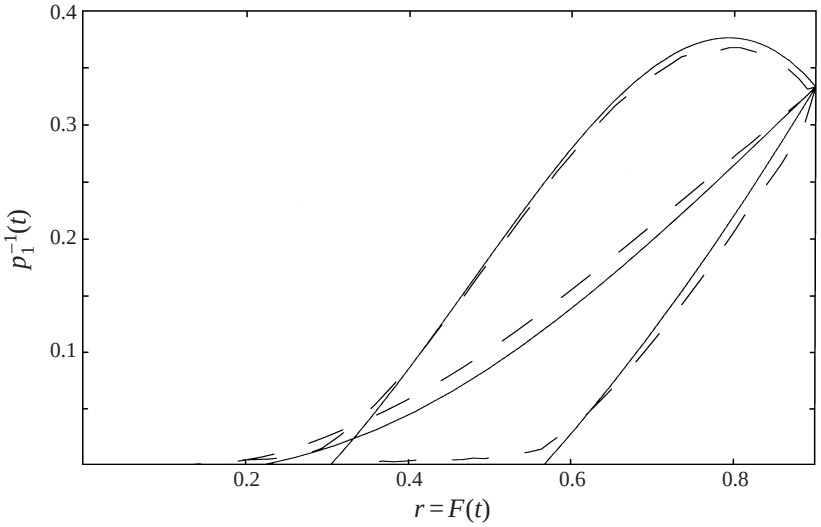

FIGURE 11. A comparison of the various physical factors controlling shock formation. The right-hand curves are for a homentropic, quiescent field. The upper curves are for a quiescent field with adverse sound speed gradient. The middle curves show the evolution of the inwardly travelling compression wave front in a collapsing gas with (the same) adverse sound speed gradient. The dashed curves indicate the results of Claw.

despite the fact that the wave is weak and undergoes dissipation in its collision with the wall.

Thus in the physical variables, contraction delays shock formation to a position closer to the bubble centre. However, one should note that contraction rapidly increases the uniform pressure of the base flow, thus one can expect stronger shocks if there is shock formation. This is beyond the scope of the present work; we refer the interested reader to Tyl & Wlodarczyk (1985).

In figure 11, we show the influence of various controlling factors in the evolution of $p_1(t)$ via (4.7). The domain is 0 to 0.9 and the wave starts from the right-hand end. The results are compared with numerical experiments with Claw to show good agreement. As before $1/p_1(t)$ is plotted against wave front position. The right-hand curves correspond to the propagation of a compression wave into a quiescent homentropic field, with $p_0 = 1$ and $a = 4$. It shocks very early. The upper curves are for an adverse sound gradient $a(r) = 4 - 3r^3$. The middle curves superpose the contraction $\alpha_0 = -2$ on the adverse sound field. As one can see the position of shock formation shifts toward the origin. Of course either a favourable sound speed gradient or an expanding base flow lead to an outward shift in the shock formation location.

4.2.2. *The case* $\gamma \neq 5/3$

This case is generally more difficult to analyse because the similarity structure no longer obtains. We make only a few remarks about this case. In kinetic theory $\gamma = 5/3$ is an upper limit (for a monatomic gas), thus γ can only be smaller than 5/3. In a contracting gas, the wave front evolution curve in scaled variables shifts to the right as γ decreases, as shown in figure 12. If γ is not far away from 5/3, the dynamics will not be very different, by continuous dependence on parameters. The physical processes remain the same as γ varies, thus our conclusion about the influences of

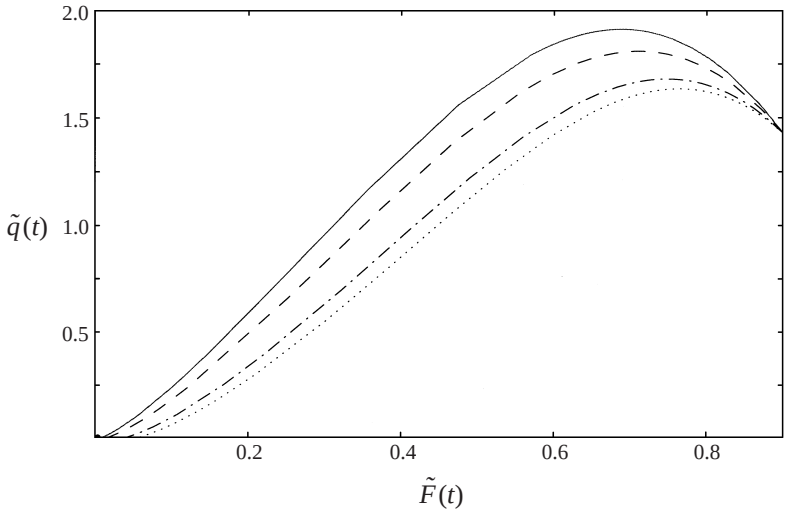

FIGURE 12. Influence of variation of γ on the evolution of an inward-travelling compression wave front, in scaled variables. Solid: $\gamma = 5/3$; dashed: $\gamma = 7/5$; dot-dashed: $\gamma = 1.1$; dotted: $\gamma = 1$.

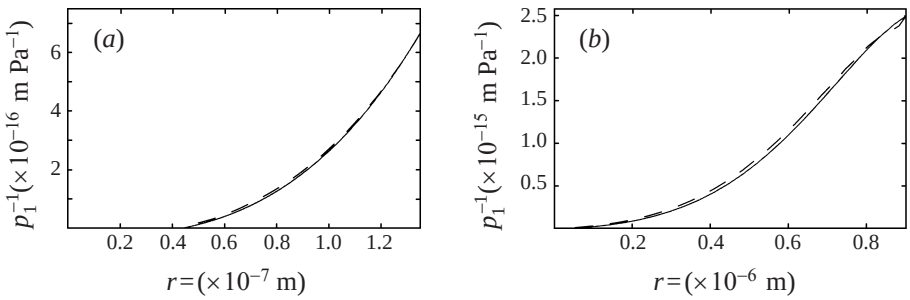

FIGURE 13. Compression wave front evolution in two cases motivated by compressible Navier-Stokes simulations of gas dynamics within a sonoluminescence bubble. In (*a*) there is the development of a shock near $r = 0.045\,\mu$m, whereas the stronger sound speed gradient in (*b*) delays the steepening to an infinitesimal shock near the centre. The latter is annihilated by diffusion in the Navier–Stokes equations as shown in figure 14. In this figure the dashed curves indicated the numerical integration of the hyperbolic conservation laws, the solid curves correspond to the analytical solution of (4.7).

different factors remains valid. Further investigation (not shown) indicates that the conclusions demonstrated in figure 11 are valid for $\gamma < 5/3$ as well.

4.2.3. *Examples based on a sonoluminescence bubble*

Finally, we consider typical data from sonoluminescence simulations conducted by Storey & Szeri (2000) to examine cases of direct relevance to sonoluminescence. Our tests are not exact duplications of the much more complicated simulations conducted, but rather a rough verification of our theory. The present theory helps one to understand when and why shocks form – or do not.

In the first case (figure 13*a*) the ambient radius of the sonoluminescence bubble is $R_0 = 4.5\,\mu$m, with driving pressure $P_A = 1.2$ atm, initial temperature $T_0 = 300$ K, driving frequency $\omega = 26.5$ kHz, and gas composition (by moles) of 86% argon and 14% water vapour. A strong compression wave of $\partial p/\partial r = 1500\,\mathrm{M\,Pa\,\mu m^{-1}}$ forms at the position $0.15\,\mu$m in radius, and it propagates into a pressure field of

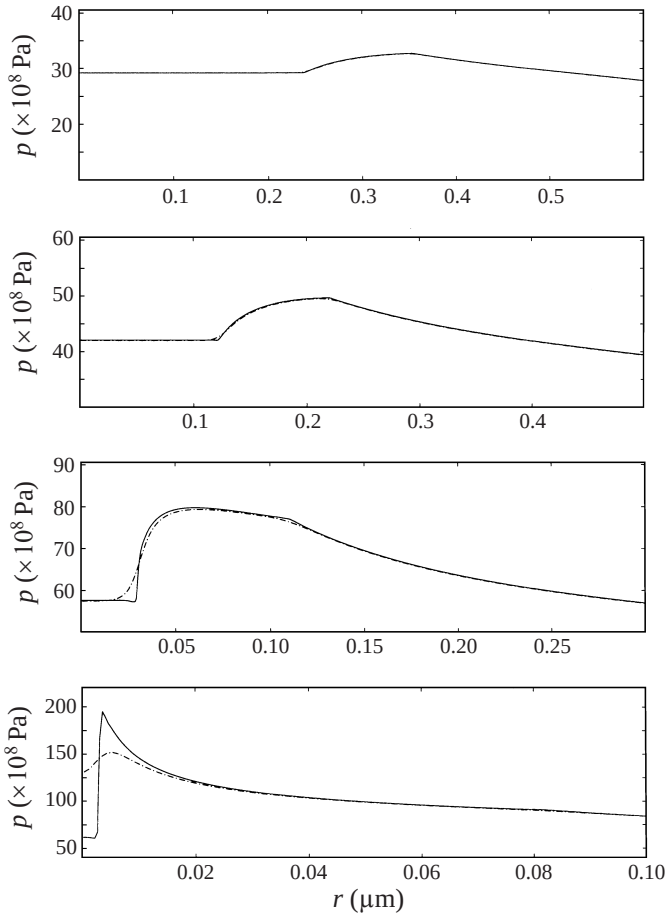

FIGURE 14. Snapshots of the travelling pressure wave in example (*b*) of figure 13. The solid curve is the calculation from the Euler equations and the dashed curve is the calculation from the full Navier–Stokes equations. The two curves are nearly identical at earlier times when the wave front is far from the centre. However, diffusion eliminates the shock that forms very close to the centre in the ideal fluid calculation.

$p_0 = 160\,\mathrm{M\,Pa}$. The contraction rate α_0 is $-4 \times 10^9\,\mathrm{s}^{-1}$; the sound velocity is nearly uniform at $1347\,\mathrm{m\,s}^{-1}$. The wave shocks at the position $r = 0.045\,\mu\mathrm{m}$.

In the second case (figure 13*b*) the ambient radius is $R_0 = 6.0\,\mu\mathrm{m}$, with driving pressure $P_A = 1.4\,\mathrm{atm}$, initial temperature $T_0 = 293\,\mathrm{K}$, driving frequency $\omega = 20.6\,\mathrm{kHz}$, and gas composition (by moles) of 68% argon and 32% water vapour. A compression wave of amplitude $\partial p/\partial r = 400\,\mathrm{M\,Pa\,\mu m}^{-1}$ takes off at position $0.9\,\mu\mathrm{m}$ into a uniform pressure field of $p_0 = 500\,\mathrm{MPa}$, with a contraction rate $\alpha_0 = -10^9\,\mathrm{s}^{-1}$ and sound speed $a_0(r) = 1407 - 962(r/10^{-6})^8\,\mathrm{m\,s}^{-1}$. Note we use an eighth-order polynomial curve fit for the sound speed that is fairly flat but with a sharp gradient near the wall. Under the influence of a strong adverse sound gradient and the contracting motion the wave forms only an infinitesimal shock close to the origin. However, this infinitesimal shock is again a theoretical artifact like the infinitesimal shocks of § 3.4.2, because it would not be observed in a full Navier–Stokes calculation; see figure 14. A detailed explanation is presented in what follows.

Both the cases show agreement with numerical experiments by Storey & Szeri. We

conducted simulations in Claw as well to verify the theory. We remark that in Storey & Szeri's simulation the model is much more complicated, yet our analytical solution captures the dominant processes that control the development of the wave fronts.

4.3. *Comments on the validity of the Euler equations*

We have shown in the spherical geometry that every inward-travelling compression wave will become a shock before it reaches the origin; however, strong enough compression waves will develop into shocks well before reaching the centre. Similarly, every rarefaction wave becomes a shock when it reaches the origin in a homentropic flow. Thus it is worthwhile considering the validity of the Euler equations as one approaches the origin of coordinates.

The Euler equations differ from the Navier–Stokes equations by neglect of the terms associated with viscosity and thermal conduction. The relevant dimensionless parameters $Re = UL/\nu$ (Reynolds number) and $RePr$ (product of Reynolds and Prandtl numbers) should both be large when the diffusion terms are neglected in favour of the convection terms. Here U is a representative velocity, L is a representative length scale for the flow, and $\nu = \mu/\rho$ is the kinematic viscosity. The Prandtl number is $Pr = \mu c_p/k$, where k is the thermal conductivity and c_p is the specific heat.

For the Reynolds number to be large means that the ratio of inertial to viscous effects is large. For the product of Reynolds and Prandtl numbers to be large means that the heat carried by the flow far exceeds the heat conducted in the flow.

We argue that the relevant length scale on which the Reynolds number should be based shrinks to zero in the case of a wave approaching the origin. Therefore the Euler equations lose validity for the case of a wave approaching the origin and the dissipation terms must be restored for an accurate solution. To examine this we shall consider the full compressible Navier–Stokes equations including viscous effects and thermal diffusion, but neglecting the small amount of heating due to viscous dissipation:

$$\rho\frac{\mathrm{D}v}{\mathrm{D}t} = -\frac{\partial p}{\partial r} + \frac{4}{3}\frac{\partial \mu}{\partial r}\left(\frac{\partial v}{\partial r} - \frac{v}{r}\right) + \frac{4\mu}{3}\left(\frac{\partial^2 v}{\partial r^2} + \frac{2}{r}\frac{\partial v}{\partial r} - \frac{2v}{r^2}\right),$$

$$\rho c_p\frac{\mathrm{D}T}{\mathrm{D}t} - \frac{\mathrm{D}p}{\mathrm{D}t} = k\left(\frac{\partial^2 T}{\partial r^2} + \frac{2}{r}\frac{\partial T}{\partial r} + \frac{1}{k}\frac{\partial k}{\partial r}\frac{\partial T}{\partial r}\right),$$

where T is the temperature. It is clear that the coordinate singularity has influence through the 'source terms' with r or r^2 in the denominator. These are the terms that eventually become indispensable and invalidate the ideal fluid approximation as a wave approaches the centre. We are only concerned with these singular diffusion terms owing to the fact that the remaining diffusive terms do not have to do with the position of the wave.

Now we consider in some detail the influence of these singular diffusion terms, by making an *a posteriori* examination using the ideal fluid calculation; that is to say, we shall investigate the self-consistency of the ideal fluid approximation. In order to estimate the importance of the singular viscous terms we simply take the ratio of the singular viscous terms to the pressure gradient; similarly we form the ratio of the singular thermal diffusion terms to the compression heating. In both cases, the ratio is between singular diffusion terms of the Navier–Stokes equation and an associated

term with similar effect from the Euler equation. The ratios are:

$$\epsilon_1 = \left[-\frac{4}{3}\frac{\mathrm{d}\mu}{\mathrm{d}T}\frac{\partial T}{\partial r}\frac{v}{r} + \frac{8}{3}\mu\left(\frac{1}{r}\frac{\partial v}{\partial r} - \frac{v}{r^2}\right)\right]\left[\frac{\partial p}{\partial r}\right]^{-1},$$

$$\epsilon_2 = \left[\frac{2k}{r}\frac{\partial T}{\partial r}\right]\left[\frac{\mathrm{D}p}{\mathrm{D}t}\right]^{-1}.$$

These parameters are generally very small when the wave is far away from the origin.

Next we evaluate ϵ_1 and ϵ_2 at the wave front, i.e. at $r = F(t)$ using the wave front expansion. This yields

$$\epsilon_1 = \left[\frac{4}{3}\frac{\mathrm{d}\mu}{\mathrm{d}T}T_1(t)\frac{v_e}{F(t)} + \frac{8}{3}\mu\left(\frac{v_1(t)}{F(t)} - \frac{v_e}{F(t)^2}\right)\right][p_1(t)]^{-1},$$

$$\epsilon_2 = \left[\frac{2k}{F(t)}T_1(t)\right]\left[-\gamma p_e\left(v_1(t) + 2\frac{v_e}{F(t)}\right)\right]^{-1}.$$

Here $T_1(t) \equiv \partial T/\partial r(r = F(t))$, and the other notation follows that of §4. We have made use of

$$\frac{1}{p}\frac{\mathrm{D}p}{\mathrm{D}t} = \gamma\frac{1}{\rho}\frac{\mathrm{D}\rho}{\mathrm{D}t} = -\gamma\left(\frac{\partial v}{\partial r} + \frac{2v}{r}\right),$$

which is the adiabatic assumption combined with the continuity equation. Note that both the numerators and the denominators of ϵ_1 and ϵ_2 contain terms that tend to infinity in the case of shock formation. However, remarkably, the ratios tend to finite limits as the wave becomes a shock. To see this we need to make use of two relations that can be derived from the wave front expansions in §4.2:

$$a_1(t) = \frac{\gamma - 1}{2}(\alpha(t) - v_1(t)) + \frac{\partial a_e}{\partial r}(r = F(t), t),$$

$$p_1(t) = -\rho_e a_e(v_1(t) - \alpha(t)).$$

We shall also use $a^2 = \gamma RT$ to relate T_1 to a_1. Finally, for the dependence of viscosity on temperature, we use simply $\mu = \mu_0 T$ with μ_0 constant (likewise for k), which is a reasonable and simple approximation at high temperature. This allows one to obtain the limits at the time of shock formation t_B:

$$\lim_{t\to t_B}\epsilon_1 = -\left[\frac{8}{3}\frac{\mu}{\rho_e a_e}\left(\frac{\gamma - 1}{2}\frac{\alpha(t)}{a_e} + \frac{1}{F(t)}\right)\right]_{r=F(t_B),\,t=t_B},$$

$$\lim_{t\to t_B}\epsilon_2 = \left[\frac{2(\gamma - 1)k}{\gamma^2 R}\frac{a_e}{F(t)p_e}\right]_{r=F(t_B),\,t=t_B}.$$

From the limiting forms, it is clear that that while other factors in the expression for ϵ_1 and ϵ_2 remain finite, the factor $F(t)^{-1}$ causes the ratios to blow up if the place of shock formation is too close to the centre. This shows that the wave front position is indeed the controlling factor in the importance of the singular diffusion terms. We conclude that the earlier a shock forms (i.e. at larger r), the better is the ideal fluid approximation inherent in the Euler equations. A shock that forms so close to the centre that ϵ_1 or ϵ_2 grow large at the time of shock formation is not well approximated as a purely hyperbolic phenomenon. In that case the diffusion terms should be restored for a correct understanding of the development of the wave.

A final figure, 15, serves to illustrate these ideas. We performed the foregoing

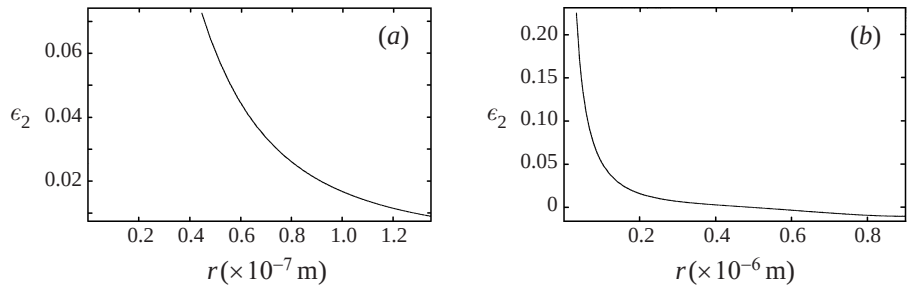

FIGURE 15. A plot of the ratio of singular thermal diffusion terms to compression heating versus wave front position r. The curve (a) corresponds to figure 13(a), and shows that the ratio remains small right up to shock formation if that occurs far enough from the origin. The curve (b) (corresponding to figure 13b) illustrates the fact that the ratio tends to infinity as the location of shock formation tends to the origin. This is an indication that the retention of the diffusive terms will have major consequence, as shown in figure 14.

analysis on the two examples of figure 13. For the case of figure 13(a), where there is the formation of an unambiguous shock at $r = 0.045\,\mu\mathrm{m}$, the parameter ϵ_2 remains small right up to the point of shock formation; one sees a shock even in a Navier–Stokes simulation (not shown). For the case of figure 13(b), which evolves only to an infinitesimal shock near the centre, ϵ_2 increases dramatically near the origin, thus indicating that the neglect of the singular thermal diffusion terms in solving the Euler equations yields a solution inconsistent with the approximation. If these terms are restored in a Navier–Stokes simulation, the shock never forms, as we have shown in figure 14. We remark that both the theory and numerical calculations indicate that thermal diffusion is always a much more prominent effect than the viscous terms in the deviation from hyperbolic behaviour. For this reason only ϵ_2 is shown in figure 15.

5. Conclusions

We have made use of a wave front expansion to explore the influence of entropy gradients (or equivalently sound speed gradients) on the evolution of compression or rarefaction waves in both Cartesian and spherical geometries. The initial compression wave propagates in an otherwise quiescent field, or in a uniformly collapsing or expanding gas. The wave is bounded by a first-order discontinuity that propagates on characteristics.

The major results are summarized as follows. In the Cartesian geometry:

(a) When waves travel into a field with a higher sound speed ahead (larger entropy), the velocity gradient of a compression wave front must exceed a critical value in order to evolve into a shock (otherwise it relaxes). Rarefaction wave fronts always relax when moving into higher sound speed areas of the flow.

(b) When waves travel into a field with lower sound speed ahead (lower entropy), all compression wave fronts evolve into shocks. Rarefaction wave fronts tend toward a permanent form of certain slope, in the case of a linearly decreasing sound speed ahead of the wave.

(c) When the quiescent field is homentropic, the classical results obtain: compression wave fronts form shocks, rarefaction wave fronts relax.

In the spherical geometry with quiescent base flow:

(a) A shock forms for any inward-travelling compression wave front for any distribution of sound speed (entropy), provided that the derivative of the sound

speed vanishes at the origin as required by the singularity. However, a sound speed field steeply decreasing outward (entropy decreasing outward) is able to delay shock formation for weak inward-travelling compression waves. When the location of shock formation is delayed close enough to the origin, diffusion would dominate its final stages of evolution, hence such an infinitesimal shock would probably not be seen in the presence of diffusion.

(*b*) Even inward-travelling rarefaction wave fronts are found to evolve into infinitesimal shocks in the homentropic case. Again, because this infinitesimal shock forms right at the origin, it would probably not be seen due to the inevitable action of diffusion. In other words, rarefaction wave fronts sharpen but not into shocks.

In a spherical geometry with a radially collapsing or expanding base flow:

(*a*) There is a fortuitous rescaling of variables that converts the problem into one with a quiescent base flow when $\gamma = 5/3$.

(*b*) A collapsing base flow delays shock formation of an inward-travelling compression wave front to closer to the centre.

(*c*) An expanding base flow accelerates shock formation of an inward-travelling compression wave front.

The motivation of this research was the gas dynamics in the interior of sonoluminescence bubbles. In Vuong *et al.* (1999) it was conjectured that a steep negative radial gradient in sound speed (entropy) could prevent the steepening of a compression wave into a shock. The evidence put forth was primarily circumstantial, based on a Navier–Stokes calculation. Now we have performed an inviscid analysis that clarifies the picture, as follows. Diffusive transport (of heat) sets up a temperature (or entropy or sound speed) gradient in the bubble by the time a compression wave is launched inward. It is by a strictly hyperbolic mechanism that this entropy gradient affects the evolution of the compression wave into a shock.

The present work has shown that it is always possible to create a shock at finite radius from a steep enough inwardly travelling compression wave front. This wave front must be steep enough so that the shock forms far enough away from the bubble centre in order not to be eliminated by diffusion. A strong enough wave front evolves into a shock even in an adverse entropy gradient, even in a radially collapsing gas.

This research was supported by a grant from the National Science Foundation Program in Theoretical Physics. The authors would like to thank Professor B. D. Storey for numerous helpful discussions.

Appendix. Simple and semi-simple waves

For initial data (i.e. non-uniform pressure and/or non-zero velocity) with compact support in an otherwise quiescent field, one can expect two waves to separate in time in the homentropic case. By virtue of (2.3) one expects a third wave (along the third set of characteristics C_0) to separate in time from initial data with compact support in a non-homentropic field.

A.1. *Homentropic flow*

A *simple wave* in the homentropic problem is a disturbance that propagates only on one set of characteristics. From (2.8), one can easily show that the slopes of the characteristics evolve according to

$$\frac{\mathrm{d}^+}{\mathrm{d}t}\,[u+a] = \frac{3-\gamma}{2}a\partial_x\Pi^-, \qquad \frac{\mathrm{d}^-}{\mathrm{d}t}\,[u-a] = -\frac{3-\gamma}{2}a\partial_x\Pi^+.$$

Hence if Π^- is uniform in a homentropic problem at $t = 0$, it is always uniform (by (2.8)). In this case there is no wave propagating on the C_- characteristics, and the C_+ characteristics are particularly simple, with constant slope determined by the initial data. It is straightforward to determine initial data that will lead only to a right-travelling wave: it must satisfy $\partial_x \Pi^- = 0$. Similar remarks apply to left-travelling waves.

A.2. *Non-homentropic flow*

In the non-homentropic case we do not have such a convenient concept as a simple wave. Nevertheless, it *is* possible to identify what characterizes (at least approximately) a flow with no left- or no right-travelling wave. These concepts are crucial to understand the steepening of the leading edge of a compression wave propagating into a non-uniform quiescent fluid.

The idea is the following. If the tendency of a signal bounded at time t between two C_+ characteristics ($x_1^+(t)$ and $x_2^+(t)$) is to travel only along $x_1^+(t)$ and $x_2^+(t)$, then the momentum between those two characteristics should be conserved. Mathematically, we seek conditions sufficient to ensure the momentum does not change:

$$\frac{\mathrm{d}}{\mathrm{d}t} \int_{x_1^+(t)}^{x_2^+(t)} \rho u \mathrm{d}x = 0.$$

One can show by constructing an integral balance of linear momentum for the region $\{x : x_1^+(t) \leqslant x \leqslant x_2^+(t)\}$, that in general the momentum in question changes at the rate

$$\frac{\mathrm{d}}{\mathrm{d}t} \int_{x_1^+(t)}^{x_2^+(t)} \rho u \mathrm{d}x = -\left[p - \rho u a\right]_{x_1^+(t)}^{x_2^+(t)} \equiv -S\big|_{x_1^+(t)}^{x_2^+(t)}.$$

The grouping $S \equiv p - \rho u a$ we shall refer to as the *flow force*, after Benjamin (Benjamin 1962, 1984; Benjamin & Lighthill 1954). This quantity is also called the total momentum flux by Lighthill (1978). To paraphrase Lighthill, S is equal to the rate of transport of momentum (here relative to the C_+ characteristics) due to: (i) the action of the pressure, and (ii) the convection by the (relative) velocity ($-a = u - (u + a)$).

Clearly, if between $x_1^+(t)$ and $x_2^+(t)$ $\Delta S = 0$ at some time t, then the momentum between the characteristics is not changing at that instant. For the momentum to be conserved over some finite interval of time, ΔS must remain zero.

To begin, S is more conveniently written $S = p\,[1 - \gamma M]$, where $M \equiv u/a$ is the Mach number. We take the derivative of S along the forward characteristics:

$$\frac{\mathrm{d}^+ S}{\mathrm{d}t} = [1 - \gamma M]\,\frac{\mathrm{d}^+ p}{\mathrm{d}t} - \frac{\gamma p}{a}\,\frac{\mathrm{d}^+ u}{\mathrm{d}t} + \frac{\gamma p u}{a^2}\,\frac{\mathrm{d}^+ a}{\mathrm{d}t}.$$

We use the field equations and the definition of entropy to obtain

$$\frac{\mathrm{d}^+ S}{\mathrm{d}t} = \left(2 - \frac{\gamma + 1}{2} M\right)\,\frac{\mathrm{d}^+ p}{\mathrm{d}t} + \frac{(\gamma - 1)}{2}\,\frac{pu}{R}\,\partial_x s. \tag{A 1}$$

Hence, along C_+, the flow force changes due to a change in the pressure p or an entropy gradient. The latter term is unavoidable in a non-homentropic flow. However, if $\mathrm{d}^+ p/\mathrm{d}t$ is zero, or small, then the flow force along C_+ is nearly constant except for changes related to the non-uniformity of the domain into which it propagates. In this case S is approximately invariant along two neighbouring C_+ characteristics. If ΔS

was zero at some initial time, then from physical principles we can expect the wave will be confined between the two C_+ characteristics.

In addition, if we evaluate (A 1) along the C_+ characteristic that defines the leading edge of a wave in an otherwise quiescent field, u and $\mathrm{d}^+u/\mathrm{d}t = -(\rho a)^{-1}\mathrm{d}^+p/\mathrm{d}t$ are zero. Hence S is absolutely invariant along this special characteristic.

By a similar argument, one can establish

$$\frac{\mathrm{d}^-S}{\mathrm{d}t} = \left(2 + \frac{\gamma+1}{2}\,M\right)\frac{\mathrm{d}^-p}{\mathrm{d}t} + \frac{(\gamma-1)}{2}\,\frac{pu}{R}\,\partial_x s. \tag{A 2}$$

Hence, if $\mathrm{d}^-p/\mathrm{d}t$ is zero, or small, then the flow force along C_- is nearly constant except for changes related to the non-uniformity of the domain into which it propagates. If S is approximately invariant along two neighbouring C_- characteristics, and if ΔS was zero at some initial time, then from the balance of linear momentum we expect such a wave to be confined between the two C_- characteristics.

Now, by use of the field equations, one can easily show that

$$\frac{\mathrm{d}^+p}{\mathrm{d}t} = \rho a\left[\frac{1}{\rho}\,\partial_x p - a\partial_x u\right], \qquad \frac{\mathrm{d}^-p}{\mathrm{d}t} = \rho a\left[-\frac{1}{\rho}\,\partial_x p - a\partial_x u\right]. \tag{A 3}$$

Hence, waves which are only right-travelling satisfy (by (A 1), (A 3))

$$a\partial_x u - \rho^{-1}\partial_x p = 0. \tag{A 4}$$

Waves which are only left-travelling satisfy (by (A 2), (A 3))

$$a\partial_x u + \rho^{-1}\partial_x p = 0. \tag{A 5}$$

We refer to such waves as *semi-simple waves.*

As we mentioned before, a general compact initial condition will separate into three waves. In the right-travelling wave, (A 4) will spontaneously be satisfied; in the separated left-travelling wave, (A 5) will be spontaneously satisfied. This is true even though neither (A 4) nor (A 5) holds true for the initial condition.

The connection between simple and semi-simple waves is established in the following manner. In a homentropic flow, we have $\partial_x s = 0$, which implies

$$\frac{2a}{\gamma-1}\,\partial_x a - \frac{1}{\rho}\,\partial_x p = 0.$$

This result changes (A 3) into

$$\frac{\mathrm{d}^+p}{\mathrm{d}t} = -\rho a^2\partial_x \Pi^-, \qquad \frac{\mathrm{d}^-p}{\mathrm{d}t} = -\rho a^2\partial_x \Pi^+.$$

Hence, by (A 1), in a homentropic flow there is no change of S along C_+ when the Riemann invariant Π^- is uniform. Likewise, by (A 2), in a homentropic flow there is no change of S along C_- when the Riemann invariant Π^+ is uniform. This recovers the result of § A.1 regarding simple waves. The idea of a semi-simple wave can be extended to the spherical case, provided that $2av/r$ is small, which obtains when r is large.

REFERENCES

Benjamin, T. B. 1962 Theory of the vortex breakdown phenomenon. *J. Fluid Mech.* **14**, 503–529.

Benjamin, T. B. 1984 Impulse, flow force and variational principles. *IMA J. Appl. Maths* **32**, 3–68.

Benjamin, T. B. & Lighthill, M. J. 1954 On cnoidal waves and bores. *Proc. R. Soc. Lond.* A **224**, 448–460.

Chu, M.-C. 1996 The homologous contraction of a sonoluminescing bubble. *Phys. Rev. Lett.* **76**, 4632–4635.

Courant, R. & Friedrichs, K. O. 1948 *Supersonic Flow and Shock Waves.* Interscience Publishers, New York.

Greenspan, H. P. & Nadim, A. 1993 On sonoluminescence of an oscillating gas bubble. *Phys. Fluids* A **5**, 1065–1067.

Landau, L. D. & Lifshitz, E. M. 1959 *Fluid Mechanics.* Pergamon.

LeVeque, R. J. 1997 Wave propagation algorithms for multi-dimensional hyperbolic systems. *J. Comput. Phys.* **131**, 327–353.

Liepmann, H. W. & Roshko, A. 1957 *Elements of Gasdynamics.* Wiley.

Lighthill, M. J. 1978 *Waves in Fluids.* Cambridge University Press.

Prosperetti, A. 1991 The thermal behaviour of oscillating gas bubbles. *J. Fluid Mech.* **222**, 587–616.

Shankar, R. & Jain, S. K. 1980 On weak discontinuities through thermally conducting and dissociating gases. *Proc. Indian Acad. Sci. (Math. Sci.)* **89**(1), 53–60.

Storey, B. D. & Szeri, A. J. 2000 Water vapour, sonoluminescence and sonochemistry. *Proc. R. Soc. Lond.* A **456**, 1685–1709.

Tyl, J. & Wlodarczyk, E. 1985 An analysis of the propagation of concentric shock wave fronts in a nonhomogeneous polytropic gas. *J. Tech. Phys.* **26**, 3–15.

Vuong, V. Q., Szeri, A. J. & Young, D. A. 1999 Shock formation within sonoluminescence bubbles. *Phys. Fluids* **11**, 10–17.

Witham, G. B. 1974 *Linear and Nonlinear Waves.* Wiley.

Zel'dovich, Ya. B. & Razier, Yu. P. 1966 *Physics of Shock Waves and High-Temperature Hydrodynamic Phenomena.* Academic.